Ti_3C_2 MXene as an excellent anode material for high performance microbial fuel cells

Da Liu,[a†] Ruiwen Wang,[a†] Wen Chang,[a] Lu Zhang,[a] Benqi Peng,[a] Huidong Li,[a] Shaoqin Liu[ab] Mei Yan*[ab] and Chongshen Guo*[ab]

*School of Life Science and Technology, Harbin Institute of Technology, Harbin 150001, China. *E-mail: yanmei@hit.edu.cn, chongshenguo@hit.edu.cn*

Key Laboratory of Micro-systems and Micro-structures Manufacturing, Ministry of Education, Harbin Institute of Technology, Harbin 150001, China.

† Da Liu and Ruiwen Wang contributed equally to this work.

Microbial community analysis

After 500 h steady and repeatable voltage output, anodes were cut into pieces and taken for DNA extraction. DNA extraction was conducted using Power Soil DNA Isolation Kit (MoBio Laboratories, Inc., Carlsbad, CA) following the manufacturer's instructions. DNA concentration was confirmed by a spectrophotometer (NanoDrop 2000c, Thermo, USA). High-throughput microbial community analysis was conducted on MiSeq platforms. Raw sequence data to NCBI Sequence Read Archive (SRA) was uploaded with accession number PRJNA428311. Universal primers 515F (5'-GTGCCAGCMGCCGCGGTTAA-3'), and 907R (5'-CCGTCAATTCCTTTGAGTTT-3') was used for PCR amplifying V4 and V5 regions of the bacterial 16S rRNA gene. PCR product was mixed and purified with Qiagen Gel Extraction Kit (Qiagen, Germany). Sequencing libraries were generated using TruSeq DNA PCR-Free Sample Preparation Kit (Illumina, USA). Individual samples were barcoded in one run of an Illumina Hiseq platform (2500, Illumina, CA) that generated 250 bp paried-end sequencing reads. OTUs were generated by sequences (analyzed by Uparse software) with ≥ 97% similarity. Phylogenetic relationship was constructed by phylogenetically assigning sequences obtained to the phylum, order, class, family and genes level using the MOTHUR program with distance level of 0.03 and confidence threshold of 97% for the phylogenetic classification. Relative abundance of a certain sample was calculated by dividing its total sequences to the total sequences.

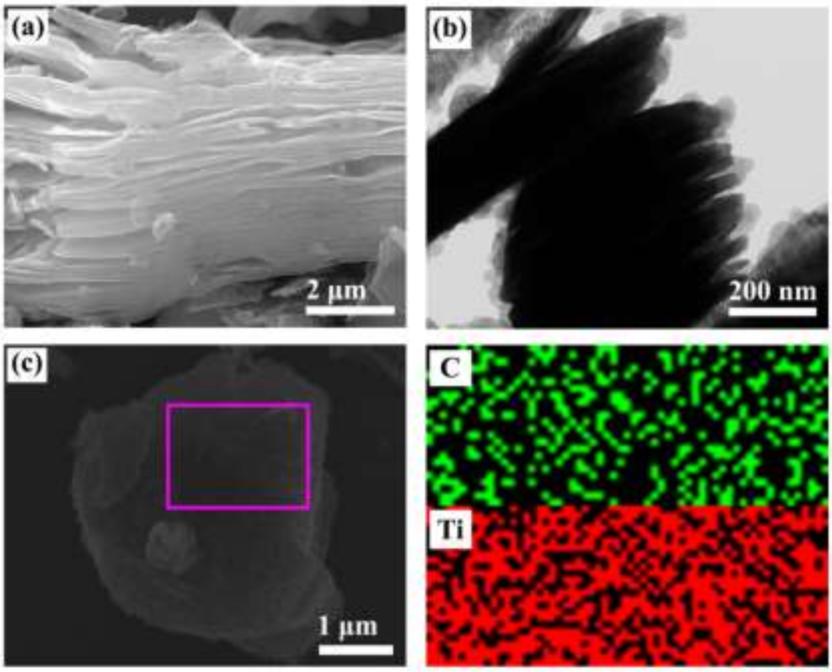

Fig. S1 (a)-(b) SEM and TEM images of multilayers Ti_3C_2 MXene. (c) SEM image and corresponding elemental mapping of C and Ti

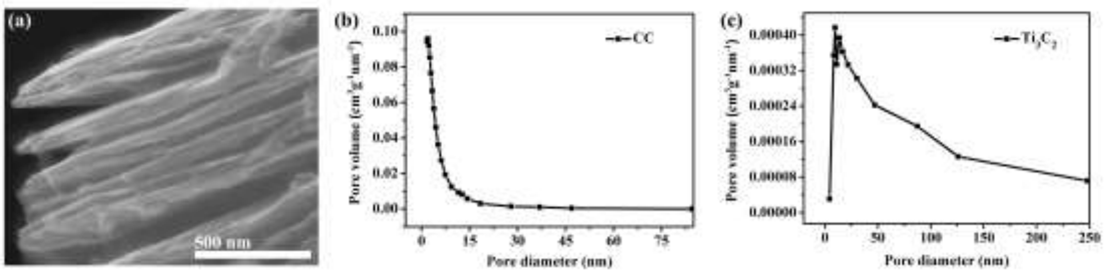

Fig. S2 (a) High-magnification SEM image of the Ti_3C_2 MXene. (b)-(c) Pore size distribution curves of the bare carbon cloth and the Ti_3C_2 MXene powder

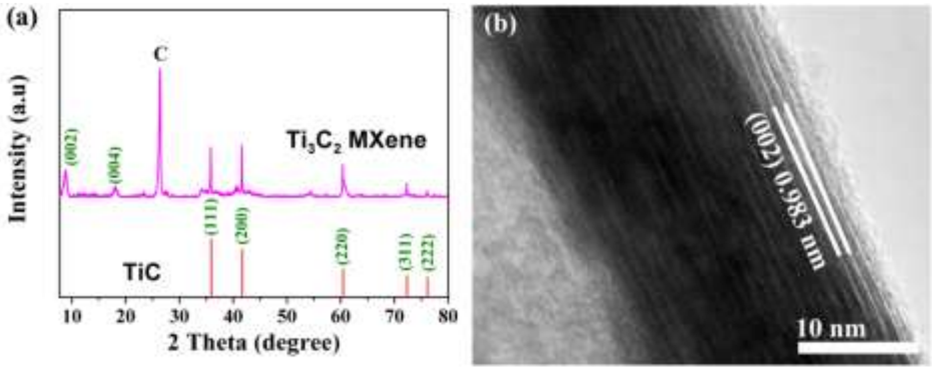

Fig. S3 (a) XRD patterns and (b) HRTEM image of Ti_3C_2 MXene

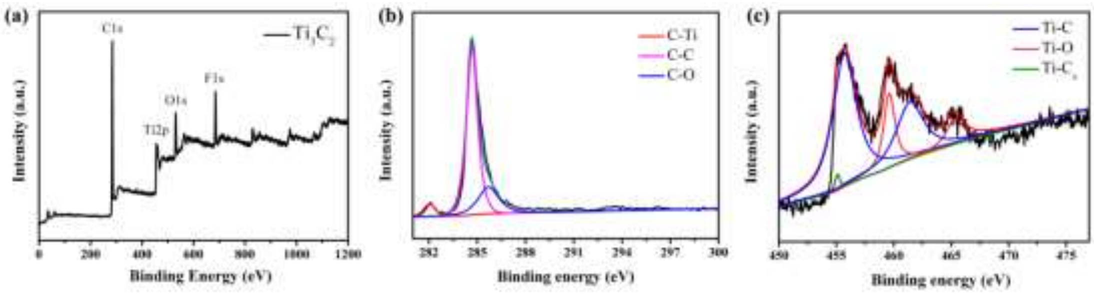

Fig. S4 (a) Full-range XPS spectra of Ti_3C_2 MXene. (b) High-resolution of C 1s and (c) Ti 2p spectra

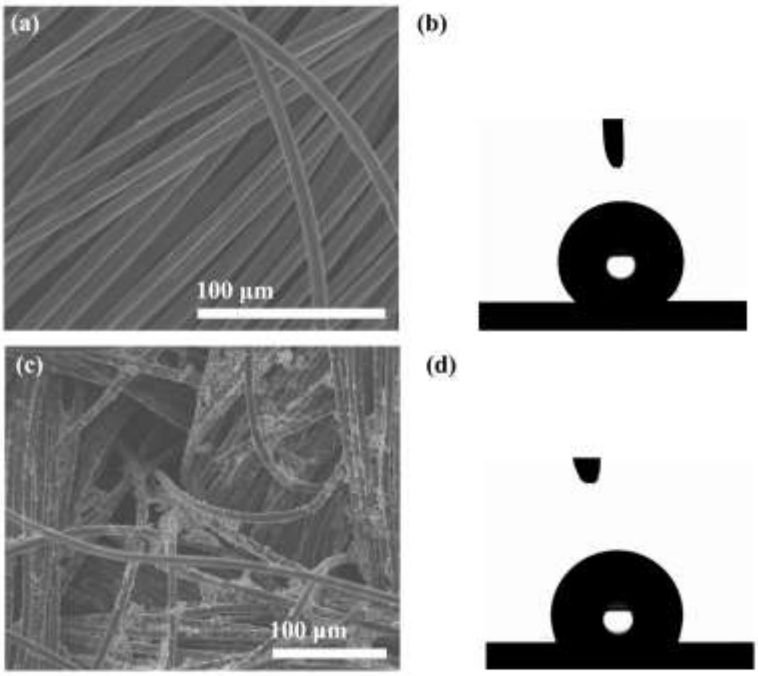

Fig. S5 (a)-(b) SEM image and contact angle (θ =140.0 °) of carbon cloth. (c)-(d) SEM image and contact angle (θ =114.8 °) of Ti_3C_2 MXene coated on the carbon cloth

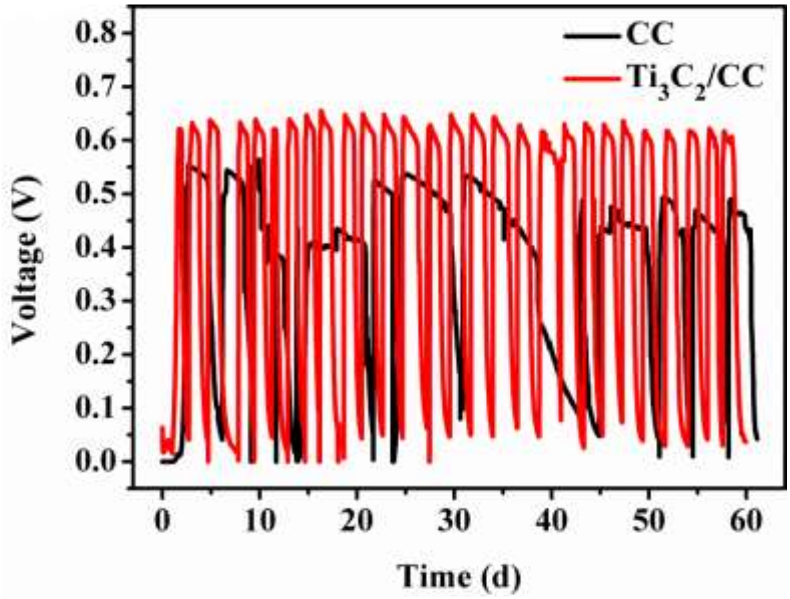

Fig. S6 The output voltage of different Ti_3C_2/CC (red)- and CC (black)-based MFCs with an external loading resistance of 1000 Ω in long-term operation

Table S1 Comparison of MFC performances with literature reports within five years

Anode	Microorganism	Feed	Configuration	Maximum power density (mW m^{-2})	Ref
N-CNTs/rGO	*S. putrefaciens* CN32	lactate	dual-chamber	1137	[S1]
Nitrogen-enriched graphitic carbon (NGC)	*S. oneidensis* MR-1	acetate	single-chamber	750	[S2]
CNT-RTIL (room temperature ionic liquid)	*Shewanella algae*	lactate	dual-chamber	245.71	[S3]
PPy/NFs/PET	*Escherichia coli*	glucose	dual-chamber	2420	[S4]
PANI/Carbon paper	*S. oneidensis* MR-1	---	dual-chamber	693±36	[S5]
Magnéli-phase titanium suboxides (MM-TiSO)	mixed	acetate	---	1541±18	[S6]
α-FeOOH	mixed	acetate	single-chamber	693±20	[S7]
Porous carbon	*E. coli*	glucose	single-chamber	1606	[S8]
rGO/MnO_2/CF	mixed	acetate	dual-chamber	2605	[S9]
TiO_2/rGO	*S. putrefaciens* CN32	---	dual-chamber	3169	[S10]
Graphene-containing foam (GCF)	*S. putrefaciens*	lactate	dual-chamber	786	[S11]
CP/GNRs/PANI	*S. oneidensis*	lactate	dual-chamber	856	[S12]
PPy/GO	*S. oneidensis* MR-1	lactate	dual-chamber	1326	[S13]

Continued

PANI-ERGNO/CC	mixed	acetate	dual-chamber	1390	[S14]
Porous graphite	*E. coli*	glucose	single-chamber	2600	[S15]
NiO/graphene	*S. putrefaciens* CN32	---	dual-chamber	3632	[S16]
FeS_2/rGO	mixed	acetate	dual-chamber	3224	[S17]
3D graphene/Pt composites	*S. oneidensis* MR-1	lactate	dual-chamber	1460	[S18]
Graphene/Au-modified carbon paper (CP/G/Au)	*S. oneidensis*	lactate	dual-chamber	508	[S19]
Graphene-layer-based graphite plate (GL/GP)	mixed	acetate	single-chamber	670±34	[S20]
PANI+G+CC	mixed	acetate	single-chamber	884±96	[S21]
Graphene microsheets	*E. coli*	glucose	single-chamber	2850	[S22]
G-CTAB-G	mixed	acetate	single-chamber	731.3	[S23]
Ti_3C_2/CC	**mixed**	**acetate**	**dual-chamber**	**3740**	**This work**

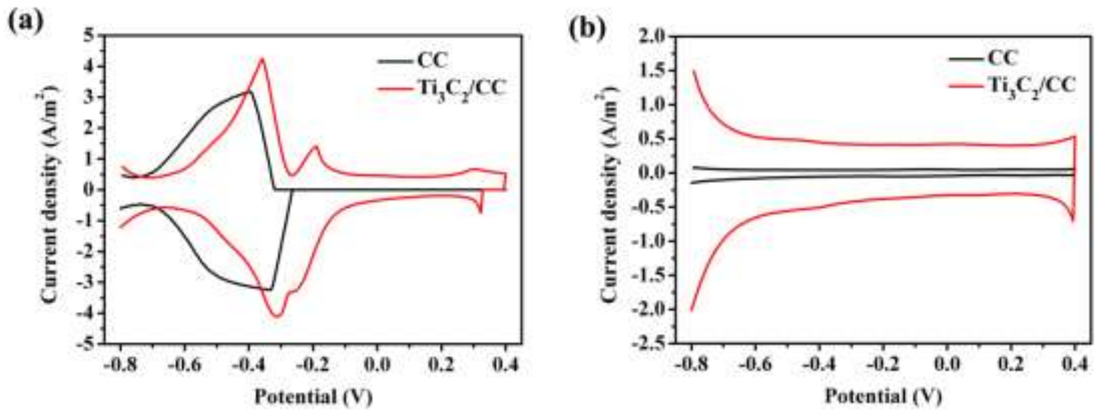

Fig. S7 DPV of (a) biofilm on Ti_3C_2/CC (red curve) and CC (black curve) anodes under turnover condition, (b) Ti_3C_2/CC (red curve) and CC (black curve) anodes without biofilm under turnover condition. Electrolyte: fresh anolyte (acetate 2 g L^{-1} in PBS with vitamin and trace element added), amplitude 60 mV, pulse width 200 ms, potential increment 6 mV, vs Ag/AgCl.

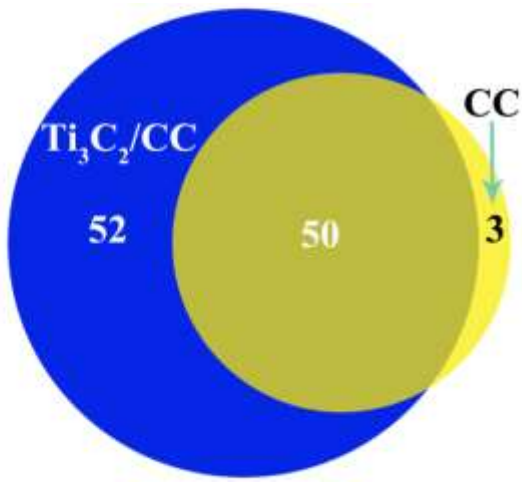

Fig. S8 The venn diagram of diversity species on Ti_3C_2/CC (blue colour, 52+50) and CC (yellow colour, 50+3) anodes.

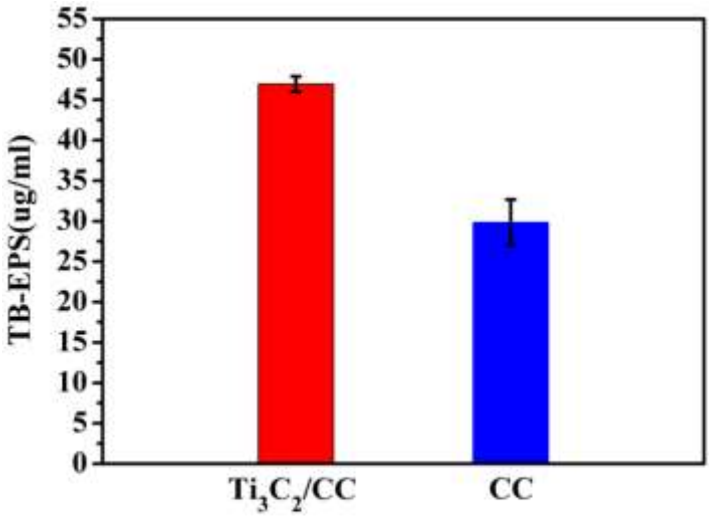

Fig. S9 The concentration of tighly bound extracellular polymeric substances (TB-EPS) in Ti_3C_2/CC and CC anode surface biofilm

References

[S1] X. S. Wu, Y. Qiao, Z. Z. Shi, W. Tang, C. M. Li, *ACS Appl. Mater. Interfaces*, 2018, **10**, 11671-11677.

[S2] S. J. You, M. Ma, W. Wang, D. P. Qi, X. D. Chen, J. H. Qu, N. Q. Ren, *Adv. Energy Mater*., 2017, **7**, 1601364

[S3] L. Mahrokh, H. Ghourchian, K. H. Nealson, *J. Mater. Chem. A*., 2017, **5**, 7979-7991.

[S4] Y. F. Tao, Q. Z. Liu, J. H. Chen, B. Wang, Y. D. Wang, K. Liu, M. F. Li, H. Q. Jiang, Z. T. Lu, D. Wang, *Environ. Sci. Technol*., 2016, **50**, 7889-7895.

[S5] R. B. Song, K. Yan, Z. Q. Lin, J. S. C. Loo, L. J. Pan, Q. C. Zhang, J. R. Zhang, J. J. Zhu, *J. Mater. Chem. A*., 2016, **4**, 14555-14559.

[S6] M. Ma, S. J. You, G. S. Liu, J. H. Qu, N. Q. Ren, *J. Mater. Chem. A*., 2016, **4**, 18002-18007.

[S7] X. H. Peng, H. B. Yu, X. Wang, N. S. J. Gao, L. J. Geng, L. N. Ai, *J. Power Sources*, 2013, **223**, 94-99.

[S8] X. F. Chen, D. Cui, X. J. Wang, X. S. Wang, W. S. Li, *Biosens. Bioelectron*., 2015, **69**, 135-141.

[S9] C. Y. Zhang, P. Liang, X. F. Yang, Y. Jiang, Y. H. Bian, C. M. Chen, X. Y. Zhang, X. Huang, *Biosens. Bioelectron*., 2016, **81**, 32-38.

[S10] L. Zou, Y. Qiao, X. S. Wu, C. X. Ma, X. Li, C. M. Li, *J. Power Sources*, 2015, **276**, 208-214.

[S11] L. Yang, S. Q. Wang, S. Q. Peng, H. M. Jiang, Y. M. Zhang, W. F. Deng, Y. M. Tan, M. Ma, Q. J. Xie, *Chem. Eur. J.*, 2015, **21**, 10634-10638.

[S12] C. Zhao, P. P. Gai, C. H. Liu, X. Wang, H. Xu, J. R. Zhang, J. J. Zhu, *J. Mater. Chem. A.*, 2013, **1**, 12587-12594.

[S13] Z. S. Lv, Y. F. Chen, H. C. Wei, F. S. Li, Y. Hu, C. H. Wei, C. H. Feng, *Electrochimica Acta*, 2013, **111**, 366-373.

[S14] J. X. Hou, Z. L. Liu, P. Y. Zhang, *J. Power Sources*, 2013, **224**, 139-144.

[S15] J. Xiong, M H. Hu, X. P. Li, H. Y. Li, X. Li, X. Liu, G. Z. Cao, W. S. Li, *Biosens. Bioelectron*., 2018, **109**, 116-122.

[S16] X. S. Wu, Z. Z. Shi, L. Zou, C. M. Li, Y. Qiao, *J. Power. Sources*, 2018, **378**, 119-124.

[S17] R. W. Wang, M. Yan, H. D. Li, L. Zhang, B. Q. Peng, J. Z. Sun, D. Liu, S. Q. Liu, *Adv. Mater*., 2018, 1800618.

[S18] S. Zhao, Y. Li, H. Yin, Z. Liu, E. Luan, Z. Feng, Z. Tang, S. Liu, *Sci. Adv*., 2015, **1**, e1500372.

[S19] C. E. Zhao, P. P. Gai, R. B. Song, J. R. Zhang, J. J. Zhu, *Anal. Methods*, 2015, **7**, 4640-4644.

[S21] L. H. Huang, X. F. Li, Y. P. Ren, X. H. Wang, *Int. J. Hydrogen Energ*., 2016, **41**, 11369-11379.

[S22] A. T. Najafabadi, N. Ng, E. Gyenge, *Biosens. Bioelectron*., 2016, **81**, 102-110.

[S23] L. X. Xue, N. Yang, Y. P. Ren, X. F. Li, Y. G. Shi, Z. Z. Hua, X. H. Wang, *J.*

Chem. Technol. Biotechnol., 2017, **92**, 157-162.